The Fe 4+/3+ redox mechanism in NaFeO 2 : A simultaneous operando Nuclear Resonance and X-ray Scattering study

Marcus Fehse, Dimitrios Bessas, Abdelfattah Mahmoud, Aliou Diatta, Raphael Hermann, Lorenzo Stievano, Moulay Tahar Sougrati

The $Fe^{4+/3+}$ redox mechanism in $NaFeO_2$: A simultaneous *operando* Nuclear Resonance and X-ray Scattering study

Dr. Marcus Fehse,[*,†,‡,¶] Dr. Dimitrios Bessas,[§] Dr. Abdelfattah Mahmoud,[‖,⊥] Aliou Diatta,[#,@] Dr. Raphael P. Hermann,[△,⊥] Prof. Lorenzo Stievano,[*,#,@,¶] and Dr. Moulay T. Sougrati[#,@,¶]

†*CIC Energigune, Parque Tecnológico de Álava, Albert Einstein 48, ED. CIC 01510, Miñano, Spain.*

‡*Faculty of Applied Sciences, Delft University of Technology, Delft, Netherlands.*

¶*Alistore European Research Institute, CNRS, Amiens, France.*

§*ESRF-The European Synchrotron, Grenoble, France.*

‖*Unit of Inorganic Materials Chemistry (GREENMAT/LCIS), Univ. Liège, Liège, Belgium*

⊥*Jülich Centre for Neutron Science JCNS and Peter Grünberg Institut PGI, JARA-FIT, Forschungszentrum Jülich GmbH, Jülich, Germany*

#*ICGM, Univ. Montpellier, ENSCM, CNRS, Montpellier, France.*

@*Reseau sur le Stockage Electrochimique de l'Energie (RS2E), CNRS, Amiens, France.*

△*Material Science and Technology Division, Oak Ridge National Laboratory, Oak Ridge, USA*

E-mail: marcus.fehse@umontpellier.fr; lorenzo.stievano@umontpellier.fr

Abstract

Simultaneous *operando* Nuclear Forward Scattering and transmission X-ray diffraction and ^{57}Fe Mössbauer spectroscopy measurements were carried out in order to investigate the electrochemical mechanism of $NaFeO_2$ vs. Na metal using a specifically designed *in situ* cell. The obtained data were analysed using an alternative and innovative data analysis approach based on chemometric tools such as Principal Component Analysis (PCA) and Multivariate Curve Resolution - Alternating Least Squares (MCR-ALS). This approach, which allows the unbiased extraction of all possible information from the *operando* data, enabled the stepwise reconstruction of the independent "real" components permitting the description of the desodiation mechanism of $NaFeO_2$. This wealth of information allows a clear description of the electrochemical reaction at the redox-active iron centres, and thus an improved comprehension of the cycling mechanisms of this material vs. sodium.

Keywords

Mössbauer spectroscopy, Chemometrics, MCR-ALS, Na-ion batteries, Nuclear Forward scattering, $NaFeO_2$

1 Introduction

Sodium ion batteries (SIB) are ideal for large-scale electrochemical storage which are not subject to weight or volume restrictions. Iron-based cathode materials are particularly interesting, since they fulfil both economical and ecological requirements [1]. In this regard, the layered transition metal oxide $NaFeO_2$ has received much interest since it was the first electrode material for SIB reversibly cycling on the $Fe^{3+/4+}$ redox couple [2]. Moreover, $NaFeO_2$ has the flattest and highest average working voltage of all single metal O3-type systems[3]. Unfortunately, its electrochemical performance deteriorates rapidly if more than

0.5 Na^+ per formula unit are extracted due to irreversible structural changes which lead to the disturbance of Na pathways caused by the migration of Fe into interslab spaces [4, 5]. Substituting Fe partially by other transition metals can suppress structural deterioration and avoid Fe migration hence increasing overall capacity and cycling stability [6, 7].

Attempts to elucidate the reaction mechanism based on *ex situ* Mössbauer spectroscopy suggest that sole Fe^{4+} formation cannot explain the overall capacity obtained and that additional charge compensation contribution must be present [8]. As a possible explanation, the contribution of both transition metal and oxygen to the charge compensation has been lately proposed [9]. In their recent in situ XAS study, Susanto *et al.* highlighted that beyond 0.5 Na^+ extraction the charge is predominantly provided by oxygen which is irreversibly released when extracting more than 0.6 Na per formula unit [10]. In other studies based on *ex situ* Mössbauer spectroscopy, it was revealed that Fe^{4+} formed during sodium/lithium extraction is unstable and spontaneously reduces back to Fe^{3+} upon open circuit storage [11, 12], underlining the importance of an *in situ* or *operando* based analytical approaches.

These observations demand for a thorough study of the evolution of the physico-chemical properties of the iron centres under realistic cycling conditions in order to closely follow the reaction mechanism and elucidate the working principle of the Fe^{4+}/Fe^{3+} redox couple. Such information can be obtained by several techniques such as X-ray absorption and ^{57}Fe Mössbauer spectroscopy, which provide element-specific core resonance information about the iron centres and can be easily applied under *in situ* conditions. On the other hand, the high degree of long range order during the phase transition between increasingly desodiated phases makes X-ray diffraction (XRD) a suitable technique to monitor the phase evolution and lattice parameter change upon desodiation reaction.

In this work, we report the application of *operando* Nuclear Forward Scattering (NFS), a spectroscopic technique based on the Mössbauer effect, to closely monitor the reaction process of $NaFeO_2$ vs. sodium. NFS, applied here for the first time to the study of battery materials, benefits from the brilliance of 3^{rd} generation synchrotron radiation sources

radiation sources, and therefore has the advantage of providing similar information but with reduced collection times (here 7 minutes per spectrum), thus opening the application of the Mössbauer effect to the study of faster reaction mechanisms than those measured conventionally (several hours per spectrum for samples non-enriched in ^{57}Fe and large amount of electrode materials).[13] Moreover, NFS allows working on samples with small sizes and is a background free method, thus enabling the collection of data with very high signal-to-noise ratios. Finally, in this experiment NFS could be coupled to *operando* transmission XRD, which was measured in parallel on the same sample during the same electrochemical processes. In this way, it was possible to measure simultaneously the evolution of both the long-range order of the material and the local physico-chemical properties of the iron centres. To validate the approach, the results of NFS are closely compared to those obtained by conventional lab-scale *operando* Mössbauer spectroscopy and X-ray diffraction applied on the same system.

2 Experimental

2.1 Material synthesis and electrode formulation

The pristine $NaFeO_2$ powders used in this work were prepared starting from 260 mg of Na_2CO_3 and 360 mg of a mixture of α-Fe_2O_3 and γ-Fe_2O_3 isotopically enriched in ^{57}Fe (95 %). The two precursors were finely ground in a mortar for 10 minutes, and then annealed in air at 600 °C for 18 hours with a heating rate of 12 °C h^{-1}. The phase purity of the pristine material was checked by laboratory X-ray diffraction (Fig. S1 table S1). Due to moisture sensitivity, the $NaFeO_2$ samples were stored and handled in a glovebox under inert atmosphere.

Electrodes with approximate diameter of 12 mm were prepared as composite self-supported pellets as previously described [14]. In short; electrodes were pasted on an aluminium foil starting from a slurry containing 85 wt.% $NaFeO_2$, 10 wt.% super-P carbon, 5 wt.% PVDF

(polyvinylideneflouride) dissolved in NMP (1-methyl-2 pyrrolidinone). The electrode used for the *operando* experiments contained $\approx 2-4\,\mathrm{mg\ cm^{-2}}$ of $NaFeO_2$.

2.2 ^{57}Fe Mössbauer spectroscopy

Operando ^{57}Fe Mössbauer spectra were measured with a source of ^{57}Co:Rh using a specially designed electrochemical cell [15] during the first desodiation-sodiation and subsequent desodiation cycle. The measurements were performed with the source and sample at room temperature with a triangular velocity waveform in the classical transmission geometry. A NaI(Tl) scintillation detector was used for the detection of the γ-rays.

2.3 Simultaneous Nuclear forward scattering and synchrotron X-ray diffraction

The *operando* NFS measurements were carried out at the nuclear resonance beamline ID18 of the European Synchrotron Radiation Facility.[16] Both the NFS and the XRD data were measured at the nuclear resonance energy (*i.e.*, about 14.412 keV) [17] related to the first excited state of ^{57}Fe. The NFS measurements utilised the time delayed nuclearly scattered radiation, which was registered with a stack of 4 avalanche photodiode detectors [18]. The time dependence of the NFS signal was detected between 15 and 160 ns after the arrival of an X-ray pulse, which in the 16 bunch operating mode of ESRF arrives every 176 ns. In this study each NFS spectrum was measured for about 7 minutes. Between two consecutive NFS spectra, a transmission X-ray diffraction (XRD) pattern was collected using the prompt electronically scattered 14.412 kev radiation (corresponding to a wavelength of 0.860 Å), which was registered using a MAXIPIX position sensitive detector [19]. Each XRD pattern was measured for about 5 seconds.

2.4 Electrochemical cycling

Both Mössbauer spectroscopy and simultaneous NFS-XRD experiments were carried out using a specifically designed *in situ* cell with two Be windows (with negligible Fe contamination, checked beforehand by conventional Mössbauer spectroscopy) allowing experiments in the transmission mode previously described elsewhere.[15] The cell was assembled in an argon-filled glove-box with a $NaFeO_2$ positive electrode, a Whatman QM-A quartz fiber separator and a sodium disc counter-electrode, using 1 M $NaClO_4$ in propylene carbonate (PC) with addition of 5 % fluoroethylene carbonate (FEC) as the electrolyte. Galvanostatic cycling with potential limitation was performed using a Biologic-VSP potentiostat at a C/n rate (expressed as 1 mol of Na reacted in n hours per mole of $NaFeO_2$).

2.5 Chemometric data analysis

The complete *operando* Mössbauer spectroscopy, NFS and XRD datasets were analysed by combining Principal Component Analysis (PCA) and Multivariate Curve Resolution-Alternating Least Squares (MCR-ALS) analysis (more details about the application of these methods to *operando* data are given in ref. [20] and, for this specific case, fig. S2). The MCR-ALS analysis for Mössbauer data set was carried out with the following constraints: non-negativity of the concentration of the components and closure (sum of the components concentrations equal to 100%). For the MCR-ALS analysis of NFS the additional constrains of unimodality, as well as the intensity of components 1, 2, 3, 4 were set to be 100% at spectra #1, 15, 20 and 33, respectively. The reconstructed pure spectral components of both techniques were subsequently fitted in a traditional way.

The components deriving from the analysis of the Mössbauer spectra were fitted with appropriate combinations of Lorentzian lines using the computer program PC-Mos II computer.[21] In this way, hyperfine parameters such as the isomer shift (δ), the electric quadrupole splitting (Δ), the full line width at half maximum (Γ) and the relative resonance areas (Area) of the different spectral components were determined. The isomer shift scale is referred to

α-iron at room temperature. The components deriving from the analysis of the NFS spectra where fitted using the software `MOTIF`.[22]

The same PCA + MCR-ALS procedure was applied to the XRD patterns collected together with NFS using the following constraints: non-negativity of the concentration and of the intensity of the components, and closure (sum of the components concentrations equal to 100%). The cells parameters of the four pure patterns obtained in this way were refined using the Le Bail method (see SI for more information).[23]

3 Results

The results shown in the following of the article were obtained in two separate *operando* experiments: a first conventional ^{57}Fe Mössbauer spectroscopy analysis, and a second synchrotron-based simultaneous NFS and XRD study. The results of these investigations are reported in the following sections and then critically discussed together.

3.1 *Operando* Mössbauer Spectroscopy

The evolution of *operando* ^{57}Fe Mössbauer spectra during first desodiation up to 3.5 V, sodiation down to 2.0 V and subsequent desodiation up to 3.8 V of $NaFeO_2$ and corresponding electrochemical signature are depicted in Fig. 1. PCA applied to the entire *operando* data set indicates that it can be reproduced by 3 orthogonal vectors (see SI for more details).

The analysis of these data required three spectral components (see SI for more details) thus excluding a biphasic reaction mechanism. Their concentration profile, see Fig. 2, reveals that component 1 is dominant at the pristine state, then completely fades away during electrochemical charge and reemerges at the end of discharge (EOD) to become primary component again. This reflects the high reversibility of the reaction when the voltage cut-off is limited to 3.5 V, as the pristine state is largely recovered after one complete cycle. Component 3 is the majority component at the end of first and second charge (EOC) reaction

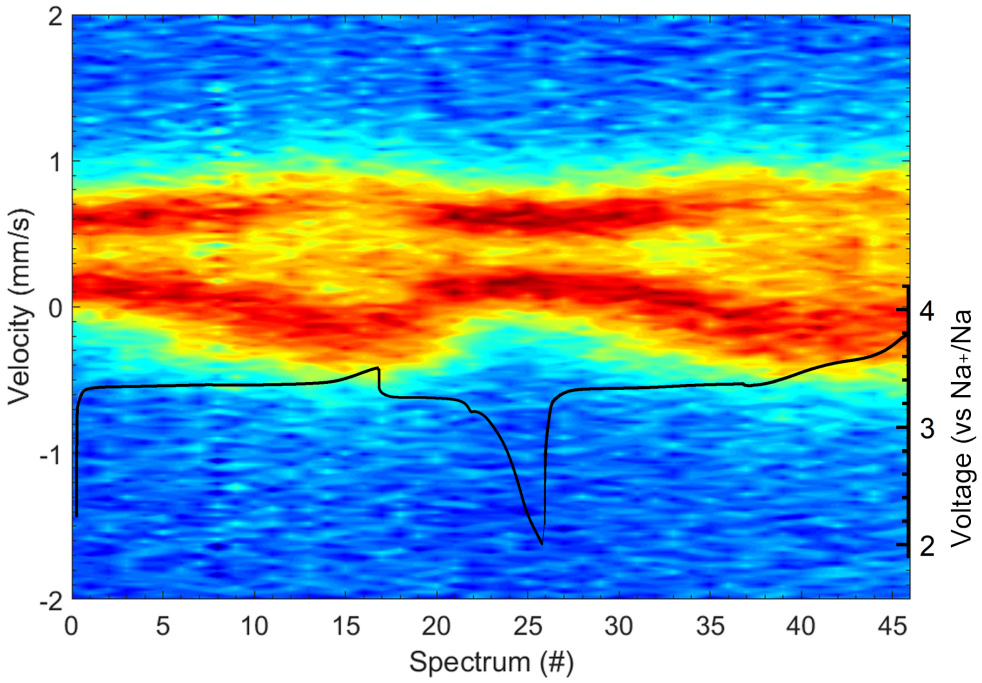

Figure 1: Evolution of *operando* ^{57}Fe Mössbauer spectra overlain with corresponding electrochemical cycling curve. First desodiation up to 3.5 V, sodiation and second desodiation reaction up to 3.8 V of $NaFeO_2$ vs. sodium.

(spectra #15 & #39). Interestingly, about halfway through each desodiation reaction step, component 2 culminates and then decreases again.

The three pure components obtained via MCR-ALS were fitted in the conventional way, the corresponding hyperfine parameters are reported in Tab. 1, and the fits are shown in Fig. 3. Component 1 corresponds to the starting component and can be fitted in straightforward fashion using single species contribution of Fe(III) with a relatively narrow quadrupole splitting Δ ($\approx$ 0.5 mm s^{-1}), well in line with literature values [2, 8]. Component 2 corresponds to the phase mix that is formed upon first and subsequent desodiation and consists of two species. Firstly, a majority of Fe(III) contribution with a larger quadrupole splitting (Δ) than observed in component 1. According to the bilinear nature of the MCR-ALS approach, this can be interpreted as either the formation of a new phase of Fe(III), or more likely a gradual increase of the Δ in the Fe(III) phase. Secondly, the apparition of a Fe(IV) minority species at significantly lower isomer shift (δ) is evinced. Component 3, which corresponds to

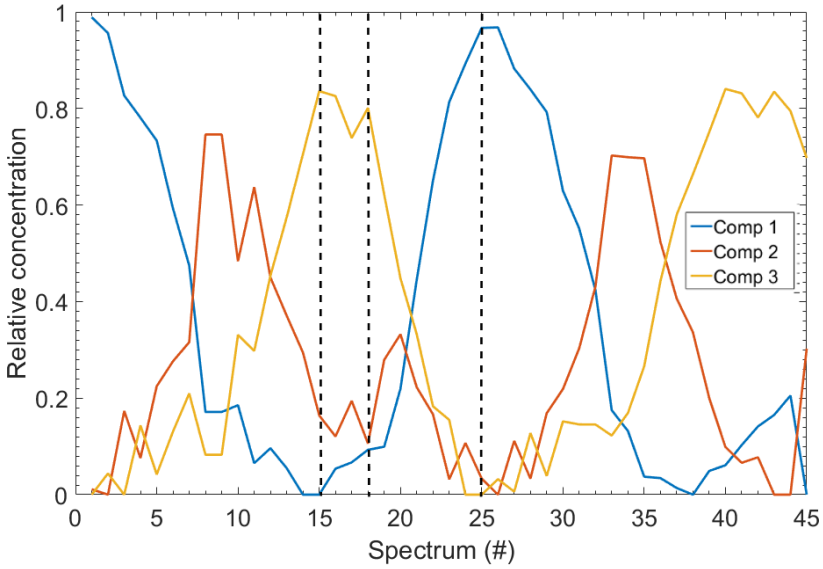

Figure 2: Concentration profile of MCR-ALS components during first 1.5 cycle of $NaFeO_2$ vs. Na. Dotted lines indicate end of charge (EOC) at #15, begin of discharge (sodiation) at #18 and end of discharge (EOD) at #25 followed by second charge (desodiation) up to 3.8 V.

the end of discharge, after completion of one electrochemical cycle can be fitted using same species as for component 2, however, with further increased quadrupole splitting Δ for both Fe(III) and Fe(IV) species. Such a strong increase in Δ was previously observed in *ex situ* Mössbauer studies and has been attributed to the distortion of the FeO_6 octahedra during desodiation [2, 11].

The gradual rise of the quadrupole splitting of the Fe(III) species and the simultaneous increase of the average oxidation state upon charge, and its reversion upon discharge are depicted in Fig. 4. It should be noted that quadrupole splitting of Fe(IV) species follows a similar trend as observed for Fe(III).

The evolution of the Mössbauer spectra beyond spectrum #38 is particularly interesting as they reflect the transformation of the cathode material upon oxidation above 3.5 V, surpassing the region of stable cycling $x \leq 0.5$. The electrochemical cycling curve reveals an additional plateau at $\approx$ 3.6 V followed by a steep slope. The chemometric analysis reveals that component 3 which reflects the formation of Fe(IV) is reaching its maximum at spectra #39. Interestingly, no further intensity increase of component 3 upon further forced oxida-

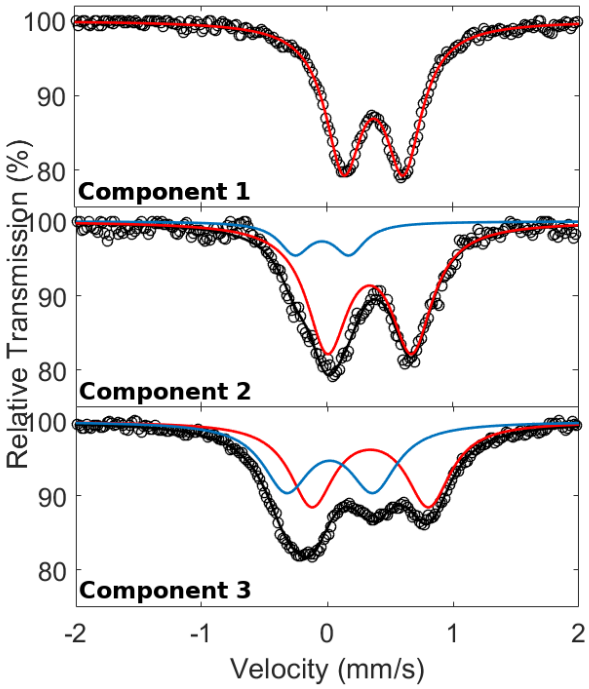

Figure 3: Mössbauer fits of pure components obtained via MCR-ALS for component 1 (pristine), component 2 (intermediate), and component 3 (EOC) in the top, centre, bottom, respectively.

tion is noticed. This suggests that the formation of Fe(IV) does not proceed beyond the 0.5 sodiation threshold, which is also reflected by the stagnation (and even a slight decrease) of the average oxidation state in Fig. 4. We can therefore conclude that the capacity obtained beyond 3.5 V is not linked to the $Fe^{+3/+4}$ redox couple. These results comfort those of Susanto *et al.*, who showed by *in situ* X-ray absorption spectroscopy that oxygen redox activity is responsible for charge compensation above 3.5 V, when more than 0.5 Na is extracted from the structure. They also suggested the formation of Fe_3O_4 caused by oxygen release at high voltage. In spite of a slight decrease of the average oxidation state, however, this observation could not be confirmed by our *in situ* data, since no clear formation of Fe(+II) species was detected.

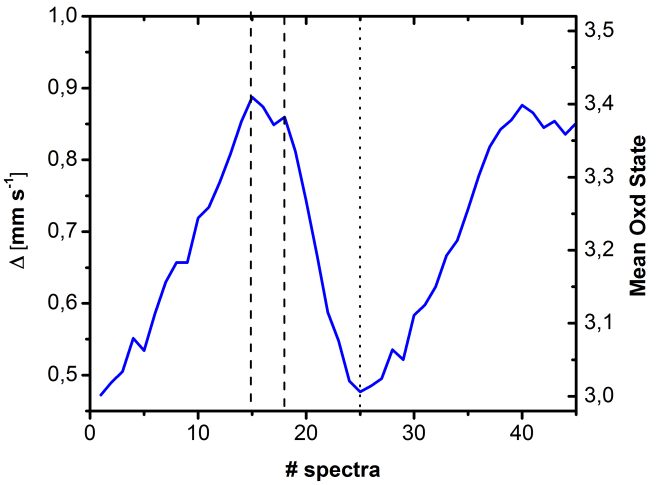

Figure 4: Evolution of Fe(III) quadrupole splitting (Δ) and Fe mean oxidation state during first 1.5 cycle of $NaFeO_2$ vs. Na. Dashed lines mark the end of first charge and the begin of first discharge at spectra # 15 and # 18 respectively. The dotted line at spectra # 25 indicates end of one complete electrochemical cycle.

3.2 Simultaneous Nuclear Forward Scattering and X-ray Diffraction

Operando NFS spectra and XRD patterns were simultaneously collected during first charge (desodiation) reaction up to 4.8 V, acquiring a total of 33 pairs of spectra and patterns (Figure 5). The NFS and XRD data sets were analysed via the chemometric approach implying PCA and MCR-ALS; in analogy with the analysis of the Mössbauer dataset (*vide supra*).

In contrast to Mössbauer spectroscopy, four independent components were identified

Table 1: ^{57}Fe Mössbauer parameters of the components derived from the MCR-ALS analysis.

Component	Species	Δ [mm s^{-1}]	δ^*[mm s^{-1}]	Γ [mm s^{-1}]	Area [%]
MCR#1	Fe(III)	0.47(1)	0.37(1)	0.35(1)	100
MCR#2	Fe(III)	0.67(1)	0.34(1)	0.40(1)	84(1)
	Fe(IV)	0.43(1)	-0.04(1)	0.30**	16(1)
MCR#3	Fe(III)	0.93(1)	0.34(1)	0.43(1)	54(1)
	Fe(IV)	0.69(1)	0.02(1)	0.45(1)	46(1)

* Isomer shift values are given relative to α-Fe at RT.
** Values without errors were fixed during the fit.

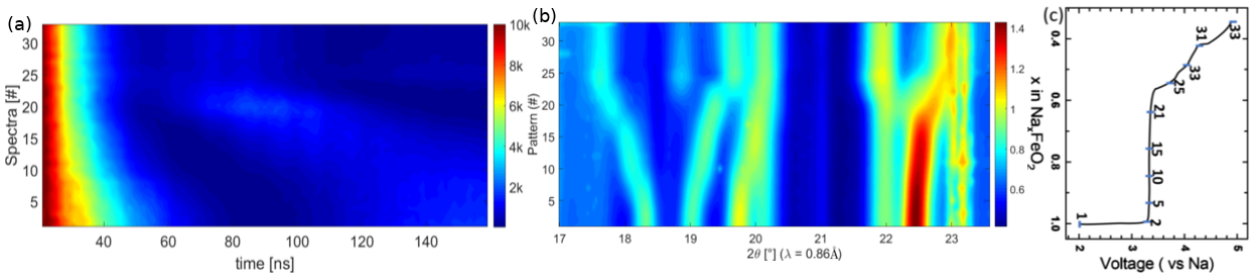

Figure 5: Evolution of (a) NFS spectra and (b) XRD pattern during first charge (desodiation) of $NaFeO_2$ up to 4.8 V vs. Na^+/Na. The NFS scattering intensity is plotted in logarithmic scale, the wavelength of angular scale is 0.86 Å. Graph (c) shows the corresponding *operando* electrochemical signature with markers for consecutively numbered data acquisition points.

via principal component analysis for both NFS and XRD (see SI for more details). Their respective concentration profiles are depicted in Fig. 6.

Component 1 reflects the pristine state of the material, whereas component 4 represents the EOC state. Component 2, and 3 are intermediate compositions. The obtained pure NFS components, shown in Fig. 7, were fitted in the conventional manner as normal NFS spectra, and the corresponding hyperfine parameters are shown in Tab. 2.

Table 2: Iron NFS fitting parameters of the MCR-ALS components.

Component	Species	Δ [mm s^{-1}]	$\Delta(\delta)$ [mm s^{-1}]*	Γ [mm s^{-1}]	Angle [°]**	Area [%]
MCR#1	Fe(III)	0.54(1)		0.35(2)	62.8(2)	100
MCR#2	Fe(III) Fe(IV)	0.780(2) 0.50(4)	0.415(8)	0.43*** 0.39***	53.6(8)	82(2) 18(2)
MCR#3	Fe(III) Fe(IV)	0.98(3) 0.63(11)	0.36(3)	0.41(2) 0.44(3)	58(2)	72(4) 28(4)
MCR#4	Fe(III) Fe(IV)	1.018(3) 0.77(1)	0.328(2)	0.51(1) 0.39***	60.0(5)	50(1) 50(1)

* Absolute value of difference in isomer shifts between two species.
** Angle refers to preferential orientation indicating texture effect.
*** Values without errors were fixed during the fit.

Component 1 can be fitted in a straight forward manner containing a single species with a quadrupole splitting (Δ) slightly higher than that observed by Mössbauer spectroscopy (MS) attributed to Fe(III), see Table 1. The other three NFS MCR components could be fitted only assuming the presence of two species with different isomer shifts. It must be

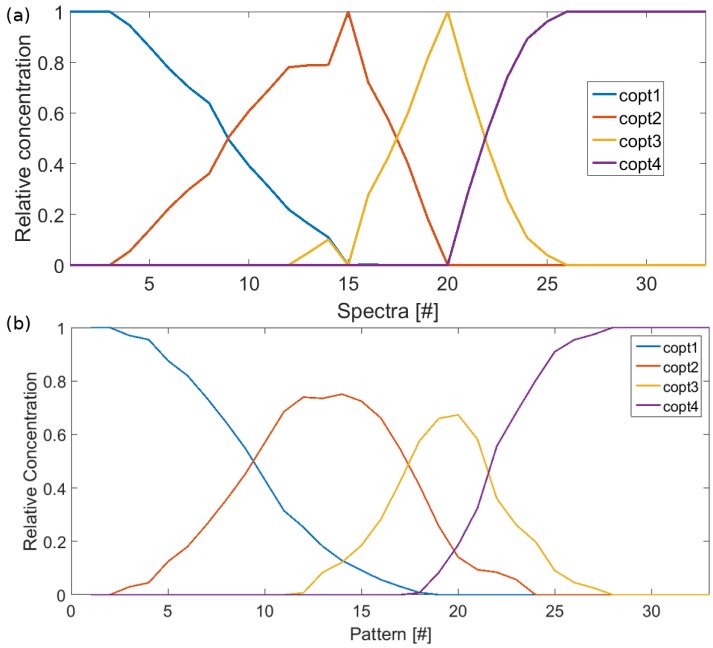

Figure 6: Concentration profile of (a) NFS and (b) XRD MCR-ALS components during first charge (desodiation) of $NaFeO_2$ vs. Na.

noted that, in contrast to MS, NFS features no reference for the isomer shift and thus only differences in isomer shift between components can be measured, but not the isomer shift itself with reference to, *e.g.*, the source or α-iron).[24].

Analogous to Mössbauer spectroscopy results, a continuous increase in quadrupole splitting of both species upon desodiation reaction is observed. The reported absolute value of difference in isomer shift ($\Delta(\delta)$) of $\approx 0.4\,\mathrm{mm\ s^{-1}}$ for component 2 and of $0.33\,\mathrm{mm\ s^{-1}}$ for component 4 are in good agreement with the differences in isomer shift of the spectral contributions of Fe(III) and Fe(IV) observed in the conventional Mössbauer spectra for the intermediate and the EOC components, which confirms the formation of Fe(IV) upon desodiation. The concentration profile shows a flat plateau for the intensity of component 4 (Figure 6) beyond spectrum #25, which coincides with a voltage above 3.5 V. This indicates that no significant changes occur to the iron doublets beyond this point. This observation is well in line with the findings of Mössbauer spectroscopy (*vide supra*) for the second charge reaction surpassing 3.5 V corresponding to spectrum $\geq$ #35.

For the linewidth (Γ) of pristine material (Component 1) a value of 0.35 is found which

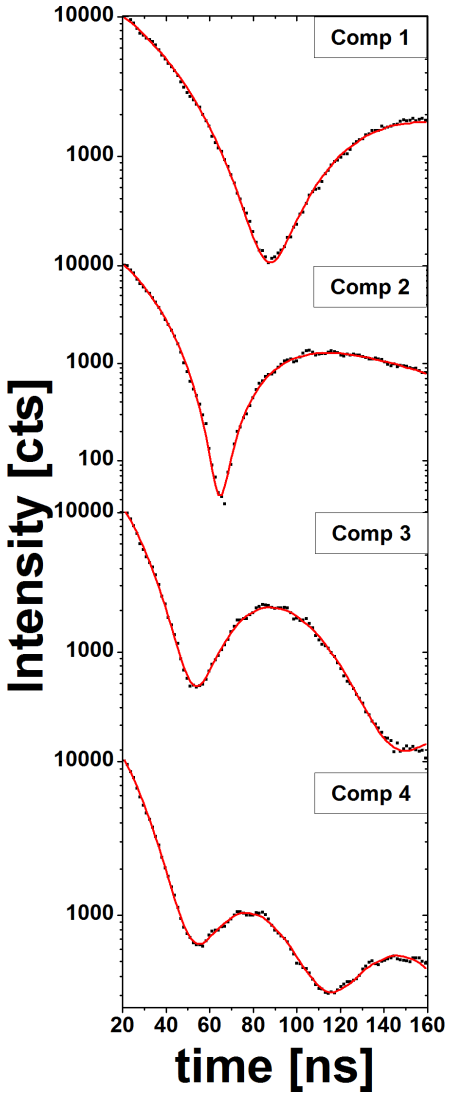

Figure 7: Fitted NFS MCR-ALS pure components during desodiation reaction of $NaFeO_2$. Black points and red lines are the pure components and the fitted data respectively.

stems almost exclusively from the effective sample thickness. For the intermediate components 2 and 3 elevated (Γ) values of $\approx 0.4\,\mathrm{mm\ s^{-1}}$ are obtained, well in agreement with component 2 of MS. At EOC, the Fe(III) contribution has a slightly higher linewidth compared to that observed by Mössbauer spectroscopy, which might be attributed to an increased disorder in the material causing a distribution of Fe(III) sites with slightly different quadrupole splittings. Nevertheless, these fitting parameters must be taken with care as linewidth strongly correlates with area weight and quadrupole splitting values.

For the angle parameter which expresses the preferential orientation effect in the material,

similar values are obtained for all components with the exception of component 2, suggesting that upon desodiation the electric field gradient in the nascent phase containing Fe(IV) has a slightly different preferential orientation from that of pristine $NaFeO_2$. As the reaction continues this difference fades out.

The evolution of the simultaneously acquired *operando* synchrotron XRD patterns upon desodiation of $NaFeO_2$ is also shown in Fig. 5(b). It depicts features at 18.31°, 19.03° and 19.06° corresponding to the (006), (101), (012) lattice planes of $NaFeO_2$, respectively. The evolution of (003) plane XRD feature at low angle 9.12° is shown in Fig. S3.

Analogously to NFS and MS, the XRD dataset was analysed by the chemometric approach using PCA and MCR-ALS, which yield four pure components (shown in Fig. S4) with the concentration profiles upon desodiation presented in Fig. 6(b). The concentration profiles are almost identical to those of NFS in terms of occurrence and succession of pure components. The four pure XRD patterns were refined using the Le Bail method (the refined cell parameters are given in Tab. S2).

The first two components could be refined using the $R\bar{3}m$ space group ($O3$-type), whereas the last two had to be refined within the monoclinic $C2/m$ space group, designated as the $O'3$ phase and typical of the partially desodiated $Na_{0.5}FeO_2$.[2] The electrochemical process seems to occur though a sequence of a monophasic-biphasic-monophasic regions. The first two components, in fact, can be linearly combined to represent the first solid solution $O3$ domain, the first one representing pristine $Na_{0.5}FeO_2$ and the second one of the same structure but with a decrease. The $O3 \rightarrow O'3$ transition is observed at about halfway through the charge process, and is followed by a second solid solution $O'3$ domain which can be obtained through the combination of components #3 and #4.

4 Discussion

The reversible extraction and insertion of Na from the $NaFeO_2$ was thoroughly monitored by *operando* Mössbauer spectroscopy and for the first charge by combined *operando* NFS-XRD. All these techniques go hand in hand, revealing the progressive oxidation of Fe(III) to Fe(IV) upon first charge. Moreover, the trend of increasing quadrupole splitting for the two iron species is mutually reflected by MS and NFS. This observation suggests an increasing distortion of the local iron environment upon extraction of sodium from the host structure. Analogously, the two techniques reflect that the electrochemical charge transfer above 3.5 V, revealed by their corresponding cycling curve, is not linked to the $Fe^{+3/+4}$ redox couple. Whether these irreversible oxidation reactions are linked to electrolyte degradation or anodic charge contribution, as recently proposed [10], cannot be answered with certainty based on our findings. Nevertheless, the formation of iron species with higher oxidation states can most certainly be excluded, in line with the findings of previous works. The increasing distortion upon oxidation is also reflected by the *operando* XRD pattern measured simultaneously with the NFS spectra. In this case, the process consists of a first solid solution domain, implying a slight decrease of the cell volume, followed by a biphasic $O3 \rightarrow O'3$ transition which occurs at about halfway through the extraction of the first 0.5 Na, *i.e.*, at a composition around $Na_{0.75}FeO_2$. This transition is followed by a further solid solution domain which ends with the extraction of 0.5 Na.

Interestingly, the application of chemometric tools to the two spectroscopic datasets leads to different number of principal components for describing the same oxidation process. The reason for this could be the more favourable signal-to-noise ratio of NFS technique compared to conventional lab-scale Mössbauer spectroscopy. Indeed, NFS data are intrinsically noise-free and do not suffer from the broadening of the experimental linewidth, which in conventional MS is the convolution of the linewidths of the source and of the absorber: in fact, the linewidth measured in NFS is that of the sample alone.

Consequently, to describe the gradual transformation of Fe(III) to Fe(IV) and their steady

increase in quadrupole splitting an additional component is needed for NFS data set. Therefore, NFS allows an improved discrimination of unresolved superimposed quadrupole doublets compared to conventional MS under similar experimental conditions.

Moreover, NFS allows for faster data collection and is particularly valuable when the concentration of Mössbauer active nuclei is low, when the size of the sample is particularly small (down to fractions of mm) or thin, and when the acquisition time is limited by the experimental framework as it is usually the case for *operando* measurements [25]. The collection of spectra in very short times permits capturing different instants of the reaction, while Mössbauer spectroscopy, collected over longer times, produces less spectra averaged over longer process fractions, and thus a lower resolution of the whole mechanism. The same is true for XRD, which thanks to the intensity of the synchrotron source provides a very good description of the redox process in relatively short measurement times.

In this regard the findings are well in line with our previous study on iron-based electrode materials in which the use of synchrotron source allowed a noticeably reduced acquisition time thanks to strongly reduced background noise compared to lab based source.[26]

5 Conclusion

In this paper, we show that Mössbauer spectroscopy and NFS are both suitable techniques to follow closely the redox reaction at the iron centres during desodiation and sodiation of $NaFeO_2$. By applying a chemometric approach for data analysis, combining PCA with MCR-ALS, it was shown that the oxidation reaction going along with the gradual extraction of sodium from the host structure involves only Fe(III) and Fe(IV) species up to the extraction of half of the sodium. After this point, the oxidation processes occurring at voltage above 3.5 V are not linked to the $Fe^{3+/4+}$ redox couple, in line with previous works suggesting the presence of anionic redox activity during the second part of the process. Ancillary XRD analyses, measured simultaneously with NFS, show that the redox reaction implies at least

three redox processes, *i.e.*, solid solution, biphasic and again solid solution. By comparing conventional Mössbauer spectroscopy and synchrotron-based NFS results, it is demonstrated here that the latter has greater accuracy for identifying characteristics of iron doublets.

Acknowledgements

Alistore-European Research Institute is gratefully acknowledged for financial support through the postdoc grant to M. Fehse. ESRF is acknowledged for providing beamtime at beamline ID18. Spanish Ministerio de Ciencia e Innovación is acknowledged for its support through the project ION-SELF (ref. PID2019-106519RB-I00). RS2E network is acknowledged for funding A. Diatta. Work by R.P.H. at Oak Ridge National Laboratory, managed by UT-Battelle, LLC, under contract DE-AC05-00OR22725 with the US Department of Energy (DOE), was sponsored by the Energy Efficiency and Renewable Energy (EERE), Vehicle Technologies Office (VTO). The technical assistance provision by Mr. J.-P. Celse is acknowledged during the beamtime at ID18.

Supporting Information Available

Characterisation of pristine $NaFeO_2$; Principal Component Analysis of the *operando* Mössbauer spectroscopy, NFS and XRD data; *Operando* XRD data analysis.

References

[1] P. Barpanda, *Chem. Mater.* **2016**, *28*, 1006–1011.

[2] Y. Takeda, K. Nakahara, M. Nishijima, N. Imanishi, O. Yamamoto, M. Takano, R. Kanno, *Mater. Res. Bull.* **1994**, *29*, 659–666.

[3] K. Kubota, S. Kumakura, Y. Yoda, K. Kuroki, S. Komaba, *Adv. Energy Mater.* **2018**, *8*, 1703415.

[4] N. Yabuuchi, H. Yoshida, S. Komaba, *Electrochemistry* **2012**, *80*, 716–719.

[5] B. Silván, E. Gonzalo, L. Djuandhi, N. Sharma, F. Fauth, D. Saurel, *J. Mater. Chem. A* **2018**, *6*, 15132–15146.

[6] X. Li, Y. Wang, D. Wu, L. Liu, S. H. Bo, G. Ceder, *Chem. Mater.* **2016**, *28*, 6575–6583.

[7] K. Kubota, T. Asari, H. Yoshida, N. Yaabuuchi, H. Shiiba, M. Nakayama, S. Komaba, *Adv. Funct. Mater.* **2016**, *26*, 6047–6059.

[8] J. Zhao, L. Zhao, N. Dimov, S. Okada, T. Nishida, *J. Electrochem. Soc.* **2013**, *160*, A3077–A3081.

[9] Y. Li, Y. Gao, X. Wang, X. Shen, Q. Kong, R. Yu, G. Lu, Z. Wang, L. Chen, *Nano Energy* **2018**, *47*, 519–526.

[10] D. Susanto, M. K. Cho, G. Ali, J. Y. Kim, H. J. Chang, H. S. Kim, K. W. Nam, K. Y. Chung, *Chem. Mater.* **2019**, *31*, 3644–3651.

[11] E. Lee, D. E. Brown, E. E. Alp, Y. Ren, J. Lu, J. J. Woo, C. S. Johnson, *Chem. Mater.* **2015**, *27*, 6755–6764.

[12] C. Dräger, F. Sigel, R. Witte, R. Kruk, L. Pfaffmann, S. Mangold, V. Mereacre, H. Ehrenberg, M. Knapp, S. Indris, *Phys. Chem. Chem. Phys.* **2018**, *21*, 89–95.

[13] J. Hastings, D. Siddons, U. van Bürck, R. Hollatz, U. Bergmann, *Phys. Rev. Lett.* **1991**, *66*, 770–773.

[14] A. Mahmoud, I. Saadoune, J. M. Amarilla, R. Hakkou, *Electrochimica Acta* **2011**, *56*, 4081 – 4086.

[15] J. B. Leriche, S. Hamelet, J. Shu, M. Morcrette, C. Masquelier, G. Ouvrard, M. Zerrouki, P. Soudan, S. Belin, E. Elkaïm, F. Baudelet, *J. Electrochem. Soc.* **2010**, *157*, A606–A610.

[16] R. Rüffer, A. I. Chumakov, *Hyperfine Interact.* **1996**, *97-98*, 589–604.

[17] Y. V. Shvyd'ko, M. Lerche, J. Jäschke, M. Lucht, E. Gerdau, M. Gerken, H. D. Rüter, H.-C. Wille, P. Becker, E. E. Alp, W. Sturhahn, J. Sutter, T. S. Toellner, *Phys. Rev. Lett.* **2000**, *85*, 495–498.

[18] A. Q. Baron, *Hyperfine Interactions* **2000**, *125*, 29–42.

[19] C. Ponchut, J. M. Rigal, J. Clément, E. Papillon, A. Homs, S. Petitdemange, *J. Inst.* **2011**, *6*, C01069–C01069.

[20] M. Fehse, A. Iadecola, M. T. Sougrati, P. Conti, M. Giorgetti, L. Stievano, *Energy Storage Materials* **2019**, *18*, 328–337.

[21] G. Grosse, *PC-Mos II*, Technische Universität München, Munich (Germany), 1st ed., **1993**.

[22] Y. V. Shvyd'ko, *Hyperfine Interactions* **2000**, *125*, 173–188.

[23] A. Le Bail, *Powder Diffr.* **2005**, *20*, 316–326.

[24] R. E. Simon, I. Sergueev, J. Persson, C. A. McCammon, F. Hatert, R. P. Hermann, *Europhys. Lett.* **2013**, *104*, 17006.

[25] A. Konjhodzic, A. Adamczyk, F. Vagizov, Z. Hasan, E. E. Alp, W. Sturhahn, J. Zhao, J. J. Carroll, *Hyperfine Interact.*, **2006**, pp. 83–89.

[26] M. Fehse, D. Bessas, A. Darwiche, A. Mahmoud, G. Rahamim, C. La Fontaine, R. P. Hermann, D. Zitoun, L. Monconduit, L. Stievano, M. T. Sougrati, *Batter. Supercaps* **2019**, *2*, 66–73.